



Materials Performance and Characterization

E. Lucon,¹ T. S. Weeks,¹ J. A. Gianetto,² W. R. Tyson,³ and D. Y. Park⁴

DOI: 10.1520/MPC20130098

Fracture Toughness
Characterization of High-
Pressure Pipe Girth
Welds Using Single-Edge
Notched Tension [SE(T)]
Specimens

VOL. 4 / NO. 2 / 2015

E. Lucon,¹ T. S. Weeks,¹ J. A. Gianetto,² W. R. Tyson,³ and D. Y. Park⁴

Fracture Toughness Characterization of High-Pressure Pipe Girth Welds Using Single-Edge Notched Tension [SE(T)] Specimens

Reference

Lucon, E., Weeks, T. S., Gianetto, J. A., Tyson, W. R., and Park, D. Y., "Fracture Toughness Characterization of High-Pressure Pipe Girth Welds Using Single-Edge Notched Tension [SE(T)] Specimens," *Materials Performance and Characterization*, Vol. 4, No. 2, 2015, pp. 55-67, doi:10.1520/MPC20130098. ISSN 2165-3992

ABSTRACT

The safety and reliability of large-diameter pipelines for the transport of fluid hydrocarbons is being improved by the development of high-strength steels, advanced weld technologies, and strain-based design (SBD) methodologies. In SBD, a limit is imposed on the applied strains rather than the applied stresses. For high-pressure pipelines, SBD requires an assured strength overmatch for the weld metal as compared to the base material, in order to avoid strain localization in the weldment during service. Achieving the required level of strength overmatch, as well as acceptable ductility and low-temperature fracture toughness, is a challenge as the pipe strength increases. Published studies show that low constraint geometries such as single-edge tension [SE(T)] or shallow-notched single-edge bend [SE(B)] specimens represent a better match to the constraint conditions of surface-breaking circumferential cracks in large-diameter pipelines during service (Shen, G., Bouchard, R., Gianetto, J. A., and Tyson, W. R., "Fracture Toughness Evaluation of High Strength Steel Pipe," *Proceedings of PVP2008, ASME Pressure Vessel and Piping Division Conference*, Chicago, IL, July 27-31, ASME, New York, 2008). However, the SE(T) geometry is not included in any of the most widely used elastic-plastic fracture mechanics (EPFM) test standards. A procedure has been developed for performing and analyzing SE(T) toughness tests using a

Manuscript received December 12, 2013; accepted for publication July 14, 2014; published online August 28, 2014.

¹ Applied Chemicals and Materials Division, NIST, Boulder, CO 80303, United States of America.

² CanmetMATERIALS, Natural Resources Canada, Hamilton, ON L8P0A1, Canada.

³ CanmetMATERIALS, Natural Resources Canada, Ottawa, ON K1A1G5, Canada.

⁴ CanmetMATERIALS, Natural Resources Canada, Calgary, AB T2P4J8, Canada.

single-specimen technique that includes formulas for calculating the J -integral and crack-tip opening displacement, as well as for estimating crack size using rotation-corrected elastic unloading compliance. Here, crack-resistance curves and critical toughness values obtained from shallow-crack SE(T) specimens ($a_0/W \approx 0.25$) are compared to shallow-crack ($a_0/W \approx 0.25$) SE(B) specimens. We believe that the SE(T) methodology is mature enough to be considered for inclusion in future revisions of EPFM standards such as ASTM E1820 and ISO 12135, although additional work is needed to establish validity limits for SE(T) specimens.

Keywords

large-diameter pipelines, high-strength steels, strain-based design, strength overmatch, SE(T) specimen, elastic compliance, elastic-plastic fracture toughness, crack resistance curves, shallow cracks

Introduction

Commonly used fracture mechanics test standards such as ASTM E1820 [1] and ISO 12135 [2] presently address the measurement of fracture toughness mainly using high-constraint laboratory specimens, such as compact tension, single-edge bend [SE(B)], and disk-shaped compact tension specimens. When used to characterize the fracture toughness properties of onshore pipelines subject to geotechnical loads, which often contain flaws subject to low-constraint loading, high-constraint specimens tend to provide conservative toughness measurements. This leads to unnecessarily high costs related to material selection and pipeline design. Specimen geometries that are characterized by less crack-tip constraint, such as single-edge tension [SE(T)] specimens, are therefore preferred for use with pipeline base metals, girth welds, and heat-affected zones.

As part of a large consolidated project on strain-based design for pipeline girth weld integrity, researchers at CanmetMATERIALS (formerly CANMET Materials Technology Laboratory) developed experimental and analytical procedures for fracture toughness testing of pipelines using SE(T) specimens [3,4], based on the use of J -integral and elastic compliance measurements from crack-mouth opening displacement (CMOD). Although a multiple-specimen method for obtaining crack resistance (J - R) curves is described in a recommended practice published in 2006 by Det Norske Veritas [5], the current investigation employed a widely popular single-specimen technique, the unloading-compliance method, originally proposed by Cravero and Ruggeri for both pin-loaded and clamped SE(T) specimens [6].

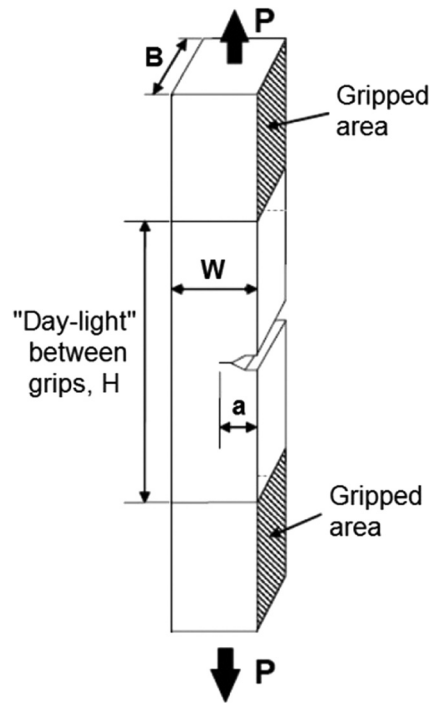
Figure 1 [5] shows a schematic of a rectangular cross-section (thickness $B = 1/2$ width W) clamped SE(T) specimen with $H = 10W$, where H is the “day-light” between grips.

Experimental Procedures

The selection of the SE(T) specimen, as well as the type of connection with the test machine (clamping) and the value $H/W = 10$, were found in previous studies to provide a reasonable match to the constraint conditions of a circumferential crack in a nuclear reactor pressure vessel [7], where conditions can be considered similar to those in a pipe subjected to tensile loading under strain-based design conditions.

FIG. 1

Clamped $B \times 2B$ SE(T) specimen with $H = 10W$ [5].



The goal of the test was to measure the J -integral fracture toughness in terms of both the critical value near the onset of ductile crack extension (J_Q) and the full crack resistance curve (J - R curve). Crack extension is monitored by measuring the elastic CMOD compliance during periodic unloading-reloading cycles.

Before the test, SE(T) specimens are precracked by fatigue from a machined notch that conforms to ASTM E1820 requirements for SE(B) notching. Fatigue precracking is achieved in three-point bending following the prescriptions of ASTM E1820, aiming at a final ratio between initial crack size and specimen width of $a_0/W \approx 0.25$ (shallow-cracked specimen). Following precracking, side-grooving of SE(T) specimens is recommended to promote straight-fronted crack propagation. Side grooves have a 45° included angle and a root radius of 0.5 mm and correspond to a reduced (net) thickness $B_N = 0.85B$ (thickness reduction = 7.5 % on each side).

The tests described in this investigation were performed at -20°C . An environmental chamber was used to control the specimen temperature to within $\pm 2^\circ\text{C}$ before and during the test. During the initial elastic portion of the force-versus-CMOD test record, several unloading/reloading sequences were performed to calculate the initial crack size and compare that value with the measured initial crack size a_0 . A force range between $0.25F_Y$ and $0.5F_Y$ was used for the initial unload/reload cycles. F_Y , the limit load for a SE(T) specimen, is given by

$$(1) \quad F_Y = B_N(W - a)\sigma_Y$$

where:

σ_Y = effective yield strength at the test temperature (average between 0.2 % offset yield strength and tensile strength),

a = current crack size,
 W = width, and
 B_N = reduced thickness.

Beyond the linear elastic range and during the course of the test, approximately 30 to 40 unloading/reloading cycles were performed to allow for crack size measurements. An unload/reload range corresponding to 25 % of the maximum force value at the beginning of the cycle (after force relaxation is complete) is typically used, in order to reduce possible hysteresis of the compliance loop [3].

After the completion of the test, the specimen was heat-treated at approximately 300°C for approximately 30 min, and the fracture surfaces were liberated by breaking the specimen in a brittle manner using liquid nitrogen. The same nine-point average technique described in ASTM E1820 was used for measuring the initial crack size and ductile crack extension (Δa_p). Both measurements were compared with analytical estimations obtained from elastic unloading compliance.

Analytical Procedure

For the calculation of the J -integral, the same formulation of ASTM E1820, where J_{el} and J_{pl} are the elastic and plastic components, respectively, of the J -integral, is used for SE(T) specimens.

$$(2) \quad J_i = J_{el,i} + J_{pl,i}$$

where i is the index of the specific unload/reload cycle, and the elastic component is given by

$$(3) \quad J_{el,i} = \frac{K_i^2(1 - \nu^2)}{E}$$

with K_i , the stress-intensity factor, given by

$$(4) \quad K_i = \left(\frac{F_i \sqrt{\pi a_i}}{\sqrt{B B_N W}} \right) \times G\left(\frac{a_i}{W}\right)$$

where:

E = plane stress Young's modulus,
 ν = Poisson's ratio at the test temperature,
 a_i = current crack size,
 F_i = force at the beginning of the unload/reload cycle, and
 $G(a_i/W)$ = function expressed as

$$(5) \quad G\left(\frac{a_i}{W}\right) = \sum_{i=1}^{12} t_i \left(\frac{a_i}{W}\right)^{i-1}$$

TABLE 1

Coefficients t_i in Eq 5 for $H/W=10$ and $0.05 \leq a/W \leq 0.95$.

i	1	2	3	4	5	6	7	8	9	10	11	12
t_i	1.197	-2.133	23.886	-69.051	100.462	-41.397	-36.137	51.215	-6.607	-52.322	18.574	19.465

Based on finite element analyses [3], the coefficients of the polynomial regression (t_i) were obtained via least-squares fitting and are provided in **Table 1**.

The plastic component of the J -integral in Eq 2 is expressed as

$$(6) \quad J_{pl,i} = \left(J_{pl,i-1} + \frac{\eta_{CMOD,i-1}}{b_{i-1}} \times \frac{A_{pl,i} - A_{pl,i-1}}{B_N} \right) \left[1 - \frac{\gamma_{LLD,i-1}(a_i - a_{i-1})}{b_{i-1}} \right]$$

where:

b_i = ligament size, given by $(W - a_i)$, and

$A_{pl,i}$ = plastic area under the force-CMOD curve.

The parameters $\eta_{CMOD,i}$ and $\gamma_{LLD,i}$ have been developed via finite element analysis (FEA) under a two-dimensional (2-D) plane strain assumption [4]. The parameter η_{CMOD} is expressed as

$$(7) \quad \eta_{CMOD} = \sum_{i=1}^{11} \phi_i \left(\frac{a_i}{W} \right)^i$$

with the coefficients ϕ_i given in **Table 2**.

The parameter γ_{LLD} is given by

$$(8) \quad \gamma_{LLD} = \eta_{LLD} - 1 - \left(1 - \frac{a_i}{W} \right) \frac{\eta'_{LLD}}{\eta_{LLD}}$$

with

$$(9) \quad \eta_{LLD} = \sum_{i=1}^{11} \psi_k \left(\frac{a_i}{W} \right)^k$$

The coefficients ψ_k are given in **Table 3**.

In Eq 8, η'_{LLD} , the first derivative of η_{LLD} , is expressed as

$$(10) \quad \eta'_{LLD} = \sum_{i=1}^{11} k\psi_k \left(\frac{a_i}{W} \right)^{k-1}$$

The equation used for the determination of crack size based on CMOD elastic compliance (C_i) measurements, valid for $0.05 \leq a/W \leq 0.95$, is

$$(11) \quad \frac{a_i}{W} = \sum_{i=1}^{10} r_i U_i$$

where

$$(12) \quad U_i = \frac{1}{\sqrt{B_e C_i E} + 1}$$

$$(13) \quad B_e = B - \frac{(B - B_N)^2}{B}$$

TABLE 2

Coefficients ϕ_i used for calculating η_{CMOD} .

i	1	2	3	4	5	6	7	8	9	10	11
ϕ_i	1	-1.089	9.519	-48.572	109.225	-73.116	-77.984	38.487	101.401	43.306	-110.77

TABLE 3Coefficients ψ_k in Eq 9 for $H/W=10$ and $0.1 \leq a/W \leq 0.7$.

k	1	2	3	4	5	6	7	8	9	10	11
ψ_k	-0.88	15.19	-35.44	18.644	18.399	-1.273	-12.756	-12.202	-4.447	5.397	14.187

and r_i are the coefficients of a polynomial least-squares fitting function [2], shown in **Table 4**.

It is interesting to note that changes in CMOD compliance (expressed as BCE ; see Eq 12) as a function of a/W for clamped SE(T) specimens are significantly larger than for SE(B) specimens, according to the formulas prescribed by ASTM E1820-11 (Fig. 2) [3].

The value of elastic compliance to be used in Eq 12 must be corrected for specimen rotation as the center of the remaining ligament moves toward the load line [6,7]:

$$(14) \quad C_{c,i} = \frac{C_i}{F_{r,i}}$$

where:

$C_{c,i}$ = rotation-corrected compliance, and

$F_{r,i}$ = rotation correction factor.

$F_{r,i}$ has been established by means of 2-D plane stress FEA [4] for a clamped SE(T) specimen with $H/W=10$ and a_0/W between 0.2 and 0.5 as

$$(15) \quad F_{r,i} = 1 - 0.165 \frac{a_0}{W} \left(\frac{F_i}{F_Y} \right)$$

It was found that for $F_i/F_Y < 1.2$, $F_{r,i}$ is largely insensitive to the material strain hardening exponent n over the range $10 \leq n \leq 30$ [4].

Material and Experimental Program

This paper reports on a number of elastic-plastic fracture toughness tests performed at -20°C on SE(T) and SE(B) specimens cut out of an X100 steel pipe of 1067-mm diameter and 14.5-mm wall thickness. The specimens were extracted in L-R orientation, and their width ($W=12.7$ mm) was close to the pipe wall thickness. All specimens had a square cross-section (*i.e.*, $W=B$) and were notched and precracked in the side that corresponded to the pipe inner diameter.

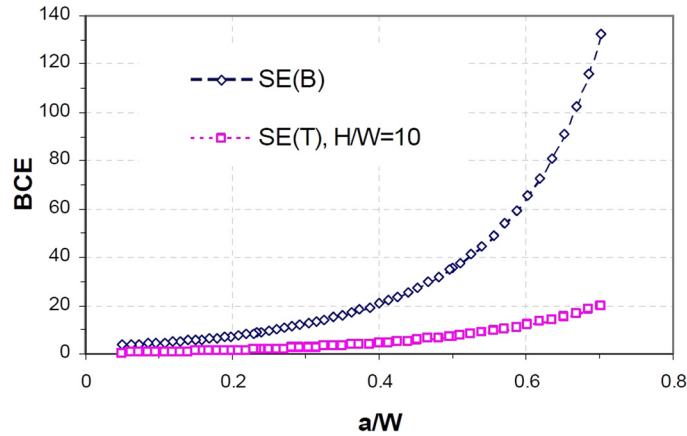
Specimens were machined from base metal (BM), single-torch girth weld metal (WM), and heat-affected zone (HAZ). Details on the welding procedures used for the preparation of the mechanized rolled welds and information about the

TABLE 4Coefficients r_i in Eq 11 for $H/W=10$.

i	1	2	3	4	5	6	7	8	9	10
r_i	2.044	-15.732	73.238	-182.898	175.653	60.93	-113.997	-113.031	8.548	142.84

FIG. 2

Relationship between BCE and a/W for SE(B) and clamped SE(T) specimens.



machining of HAZ specimens are provided in Ref 8. Only SE(B) specimens were used to characterize the BM.

The steel investigated was API 5L-X100, ASTM Grade 690; its tensile properties are provided in Table 5. For the analysis of HAZ tests, the tensile properties of the WM (higher than those of the BM, and therefore more conservative for fracture toughness analyses) were used.

Prior to fatigue precracking of WM specimens, local compression was used to avoid uneven crack fronts resulting from residual stresses in the WM. The ligament below the machined notch was compressed up to a total plastic strain not exceeding 1 % of the specimen thickness, in accordance with BS 7448-2:1997 [9]. This has a negligible effect on fracture toughness measurements, but it has a beneficial effect on the straightness of the fatigue crack front (Fig. 3).

All SE(T) specimens and SE(B) $B \times B$ specimens were fatigue precracked to a shallow initial target crack size $a_0 = 3$ mm ($a_0/W = 0.24$).

The test matrix is presented in Table 6.

Test Results

All the tests performed were analyzed in accordance with the procedures for J - R curve testing prescribed by ASTM E1820-11^{e1} [1], including the adjustment of the calculated initial crack size by fitting all (J_i, a_i) pairs before maximum force with the following equation:

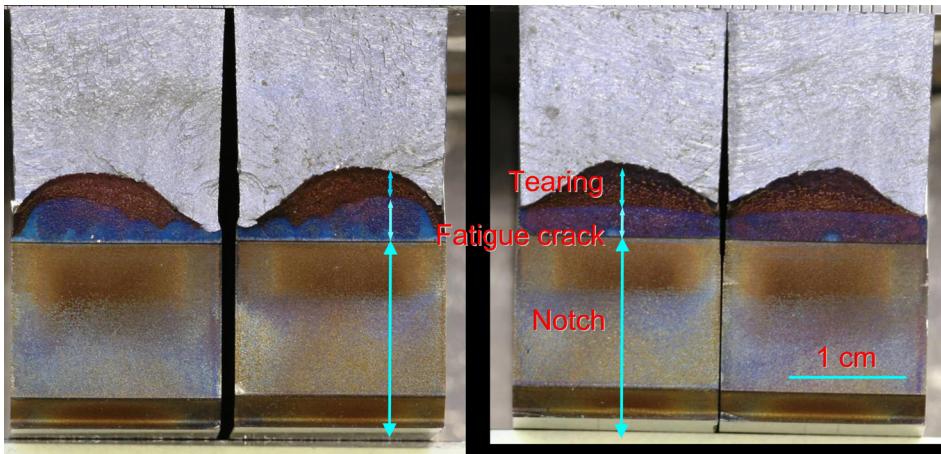
$$(16) \quad a_i = a_{0q} + \frac{J_i}{2\sigma_Y} + BJ_i^2 + CJ_i^3$$

TABLE 5

Yield and ultimate tensile strengths of X100 pipe steel measured at room temperature.

Material	σ_{YS} , MPa	σ_{UTS} , MPa
BM	679	804
WM	801	912

FIG. 3 Effect of local compression on fatigue crack front straightness: comparison between the results of precracking a weld metal SE(T) specimen without (left) and with (right) prior local compression.



where:

a_{0q} = adjusted initial crack size, and

B, C = fitting constants.

In the case of apparent negative crack extension (which occurred in most tests; see an example in **Fig. 4**), all data points preceding the minimum calculated crack size were excluded from the regression.

While all BM and WM specimens exhibited fully ductile behavior at -20°C , several HAZ specimens failed in a brittle manner. The occurrence of brittle fracture, sometimes associated with pop-in behavior, was much more frequent for SE(B) specimens (100 % of tests; an example is shown in **Fig. 5**) than for SE(T) specimens (only one test out of six). This can be attributed to the higher degree of crack-tip constraint and stress triaxiality in SE(B) tests, which promotes the occurrence of unstable fracture when the crack reaches a region with brittle microstructure near the fusion line.

CRACK SIZE MEASUREMENTS AND ESTIMATIONS

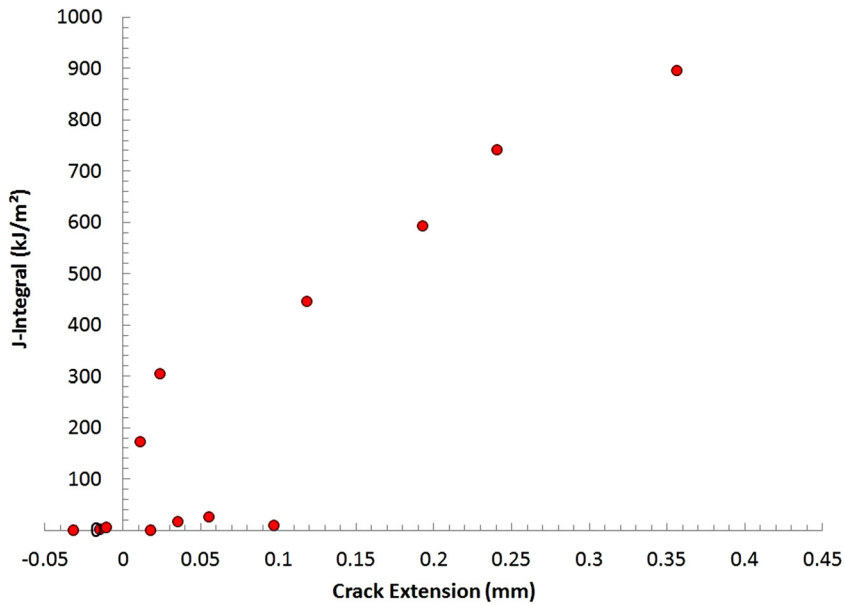
As reported separately by Park et al. [10], compliance-based predictions agreed with optically measured crack sizes for both specimen types and all materials tested. For

TABLE 6

Test matrix (all tests performed at -20°C).

Material	Specimen Type	Number of Tests
BM	SE(B)	5
WM	SE(B)	6
	SE(T)	6
HAZ	SE(B)	5
	SE(T)	6

FIG. 4 Example of apparent negative crack extension during the early stages of an SE(T) test.



BM and WM tests, measured crack sizes met the requirements of ASTM E1820, whereas in HAZ specimens the overmatching strength of the WM resulted in asymmetrical deformation at the crack tip and led to biased crack growth and different apparent crack lengths on the BM and WM sides. This occurs because the crack tends to preferentially grow in the BM side, as shown by the example provided in Fig. 6.

FIG. 5

Example of pop-in behavior observed on an SE(B) specimen of HAZ material.

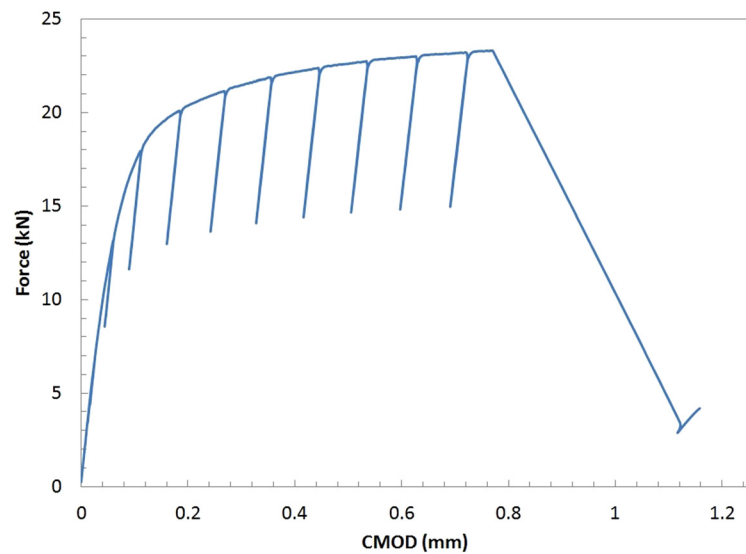
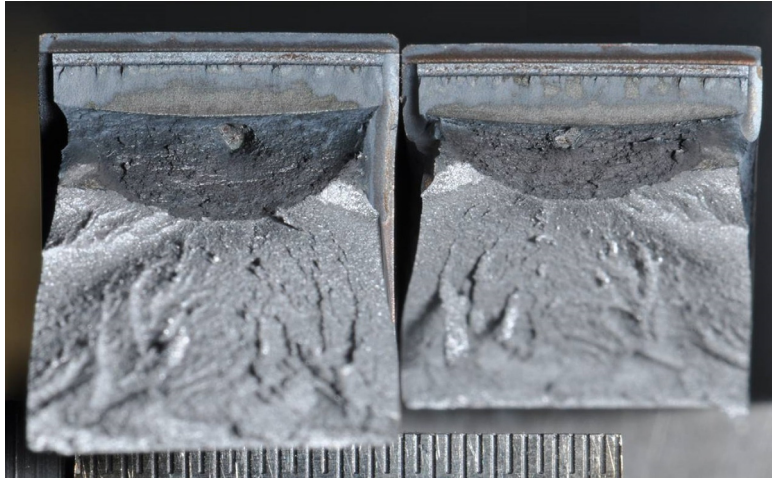


FIG. 6

Example of asymmetric ductile crack extension in an SE(T) specimen of HAZ material.



The physical crack extensions estimated from elastic compliance tended to underestimate the Δa_p values for both SE(B) [Fig. 7(a)] and SE(T) [Fig. 7(b)] specimens. The underestimation was particularly pronounced for SE(T) specimens; see Fig. 7(b). Similar observations have been reported by other authors for shallow-cracked SE(B) specimens [11,12].

MATERIAL EFFECTS ON CRACK RESISTANCE CURVES

The J - R curves presented in Fig. 8 show that the WM had significantly less resistance to crack propagation than BM or HAZ samples. Microstructural investigations, documented elsewhere [10], have shown a much greater amount of voids and microvoids in the weld microstructure, resulting in lower slopes of the J - R curves measured from WM specimens. The greater amount of voids and microvoids might be a result of porosity, or it might derive from void growth from inclusions in the fracture process zone.

FIG. 7 Comparison between compliance-based estimations and measurements of physical crack extensions for (a) SE(B) specimens and (b) SE(T) specimens.

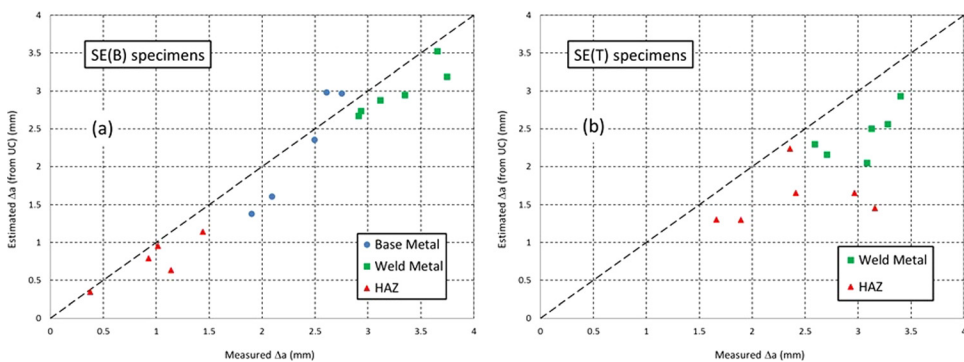
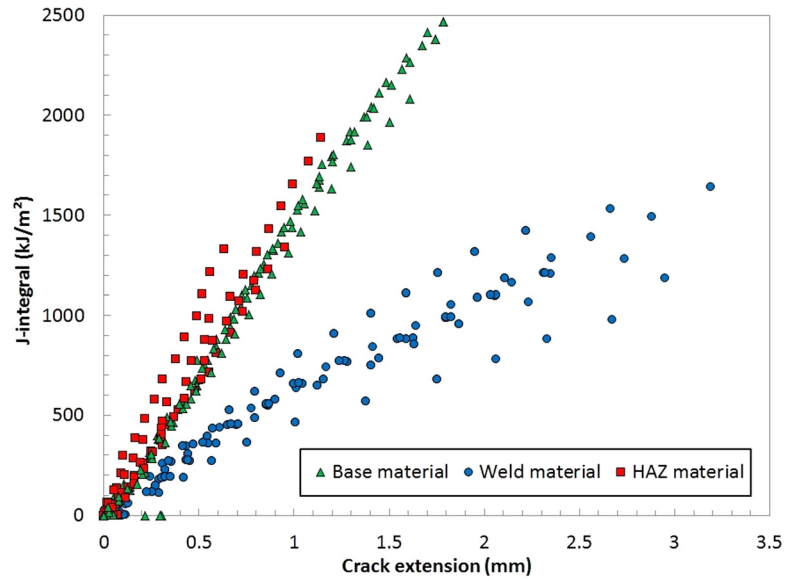


FIG. 8

J - R curves obtained from shallow-notch SE(B) specimens of base, weld, and HAZ materials.



CRACK-TIP CONSTRAINT EFFECTS ON CRACK RESISTANCE CURVES AND INITIATION TOUGHNESS

Crack-tip constraint significantly affects both crack initiation (J_Q) and the resistance to crack propagation (J - R curve), as shown in Fig. 9 by the comparison between SE(T) and SE(B) test results for WM specimens. The lower stress triaxiality at the crack tip in SE(T) specimens delays crack initiation and enhances crack growth resistance. This is consistent with the effect reported elsewhere [10] in comparisons of specimens with shallow ($a_0/W \approx 0.25$) and deep ($a_0/W \approx 0.5$) cracks.

FIG. 9

Comparison between shallow-notch SE(T) and SE(B) J - R curves for weld metal specimens.

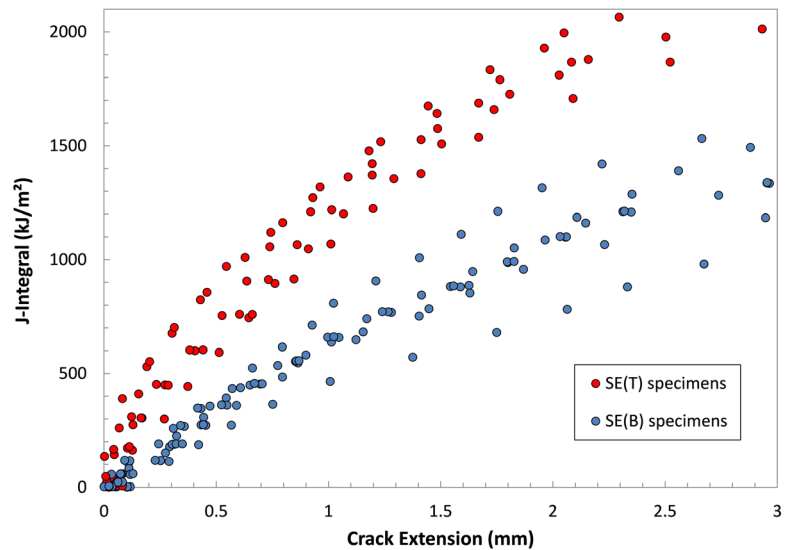
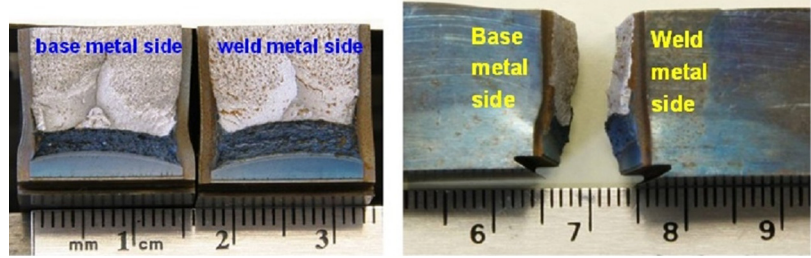


FIG. 10

Asymmetrical deformation and crack extension observed on an SE(T) HAZ specimen.



ADDITIONAL OBSERVATION: ASYMMETRICAL DEFORMATION IN HEAT-AFFECTED ZONE SPECIMENS

During HAZ tests, the BM side undergoes larger deformations than the WM side, due to the overmatching of tensile properties that causes crack extension to appear larger on the WM side (Fig. 10). In other words, the crack tends to grow preferentially into the base material. The asymmetric deformation behavior is more pronounced in SE(T) than SE(B) specimens, because of the higher stress gradient ahead of the crack tip in SE(B) specimens.

As a consequence, for several specimens the measured final crack size and the ductile crack extension fulfilled the requirements of ASTM E1820 on the WM side, but not on the BM side.

Conclusion

From a procedure/standards point of view, SE(T) testing appears robust and mature enough to be considered for incorporation into future revisions of fracture toughness standards, such as ASTM E1820 and ISO 12135. However, additional work is needed to establish and qualify the specimen measuring capacity (J_{\max}) and the crack extension limit (Δa_{\max}) for the SE(T) geometry.

ACKNOWLEDGMENTS

This work is part of a research project jointly performed by CanmetMATERIALS and NIST and sponsored by the U.S. Department of Transportation – Pipeline and Hazardous Materials Safety Administration and Pipeline Research Council International. The project was aimed at characterizing the mechanical properties of single-torch and dual-torch girth welds from X100 pipes.

References

- [1] ASTM E1820-13: Standard Test Method for Measurement of Fracture Toughness, *Annual Book of ASTM Standards*, ASTM International, West Conshohocken, PA, 2011.
- [2] ISO 12135:2002, “Metallic Materials—Unified Method of Test for the Determination of Quasistatic Fracture Toughness,” International Organization for Standardization, Geneva, Switzerland, 2002.
- [3] Shen, G., Gianetto, J. A., and Tyson, W. R., “Development of Procedure for Low-constraint Toughness Testing Using a Single-specimen Technique,” *MTL Report No. 2008-18(TR)*, CANMETMaterials, Ottawa, Canada, 2008.

- [4] Shen, G. and Tyson, W. R., "Crack Size Evaluation Using Unloading Compliance in Single-specimen Single-edge Notched Tension Fracture Toughness Testing," *J. Test. Eval.*, Vol. 37, No. 4, JTE102368, 2009.
- [5] Recommended Practice DNV-RP-F108, "Fracture Control for Pipeline Installation Methods Introducing Cyclic Plastic Strain," Det Norske Veritas, Høvik, Norway, 2006.
- [6] Cravero, S. and Ruggieri, C., "Estimation Procedure of J-resistance Curves for SE(T) Fracture Specimens Using Unloading Compliance," *Eng. Fract. Mech.*, Vol. 74, 2007, pp. 2735–2757.
- [7] Joyce, J. A. and Link, R. E., "Effect of Constraint on Upper Shelf Fracture Toughness," Reuter, W., Underwood, J. H., and Newman, J. C., Eds., *Fracture Mechanics, ASTM STP 1256*, ASTM International, Philadelphia, 1995, pp. 142–177.
- [8] Park, D.-Y., Tyson, W. R., Gianetto, J. A., Shen, G., and Eagleson, R. S., "Mechanical Properties and Microstructure of Weld Metal and HAZ Regions in X100 Single and Dual Torch Girth Welds," *Proceedings of IPC 2010, the 8th International Pipeline Conference*, Calgary, AB, Canada, Sept. 27-Oct 1, ASME, New York, 2010.
- [9] BS 7448-2:1997, "Fracture Mechanics Toughness Tests. Method for Determination of K_{Ic} , Critical CTOD and Critical J Values of Welds in Metallic Materials," British Standards Institution, London, 1997.
- [10] Park, D. Y., Tyson, W. R., Gianetto, J. A., Shen, G., Eagleson, R. S., Lucon, E., and Weeks, T., "Development of Optimized Welding Solutions for X100 Line Pipe Steel—Small Scale Low Constraint Fracture Toughness Test Discussion and Analysis," *Topical Report No. 278-T-08*, CanmetMATERIALS Technology Laboratory, Ottawa, Canada, 2011.
- [11] Joyce, J. A., Hackett, E. M., and Roe, C., "Effects of Crack Depth and Mode Loading on the J-R Curve Behavior of High Strength Steel," Hackett, E. M., Schwalbe, K.-H., and Dodds, R. H., Eds., *Constraint Effects in Fracture, ASTM STP 1171*, ASTM International, Philadelphia, 1993, pp. 239–263.
- [12] Mathias, L., Sarzosa, D., and Ruggieri, C., "Effects of Specimen Geometry and Loading Mode on Crack Growth Resistance Curves of a High-strength Pipeline Girth Weld," *Int. J. Pressure Vessel Piping*, Vols. 11–112, 2013, pp. 106–119.